Supporting Information for "Investigating the Lid Effect in the Generation of Ocean Island Basalts"

S. Jiang[1], R. Hawkins[1], M.J. Hoggard[1], D.R. Davies[1], I.H. Campbell[1]

[1]Research School of Earth Sciences, Australian National University, Canberra, ACT 2601, Australia

Contents of this file

1. Figures S1 to S11: include information about lithospheric thickness from plate models, magma evolution processes from fractionation and reverse-fractionation calculations, model evidence calculation results and associated examples, and OIB temperatures from various geochemical constraints.

2. Tables S1 to S6: include information about lithospheric thickness evaluated from different models and λ_2 values from a two-phase melting model.

March 28, 2024, 5:21am

References

Abdel-Monem, A., Fernandez, L., & Boone, G. (1975). K-Ar ages from the eastern Azores group (Santa Maria, São Miguel and the Formigas islands). *Lithos*, *8*(4), 247–254.

Ariskin, A. A., Frenkel, M. Y., Barmina, G. S., & Nielsen, R. L. (1993). COMAG-MAT: a Fortran program to model magma differentiation processes. *Computers & Geosciences*, *19*(8), 1155–1170.

Ball, P., White, N., Maclennan, J., & Stephenson, S. (2021). Global influence of mantle temperature and plate thickness on intraplate volcanism. *Nature Communications*, *12*(1), 2045.

Bao, X., Lithgow-Bertelloni, C. R., Jackson, M. G., & Romanowicz, B. (2022). On the relative temperatures of Earth's volcanic hotspots and mid-ocean ridges. *Science*, *375*(6576), 57–61.

Calvert, A. T., Moore, R. B., McGeehin, J. P., & da Silva, A. M. R. (2006). Volcanic history and ^{40}Ar/^{39}Ar and ^{14}C geochronology of Terceira Island, Azores, Portugal. *J. Volcanol. Geotherm. Res.*, *156*(1-2), 103–115.

Camps, P., Henry, B., Prevot, M., & Faynot, L. (2001). Geomagnetic paleosecular variation recorded in Plio-Pleistocene volcanic rocks from Possession Island (Crozet Archipelago, southern Indian Ocean). *J. Geophys. Res.*, *106*(B2), 1961–1971.

Caplan-Auerbach, J., Duennebier, F., & Ito, G. (2000). Origin of intraplate volcanoes from guyot heights and oceanic paleodepth. *J. Geophys. Res.*, *105*(B2), 2679–2697.

Caroff, M., Maury, R. C., Vidal, P., Guille, G., Dupuy, C., Cotten, J., . . . Gillot, P.-Y. (1995). Rapid temporal changes in ocean island basalt composition: Evidence from

an 800 m deep drill hole in Eiao Shield (Marquesas). *J. Petrol.*, *36*(5), 1333–1365.

Carracedo, J. C., Day, S., Guillou, H., Badiola, E. R., Canas, J., & Torrado, F. P. (1998). Hotspot volcanism close to a passive continental margin: the Canary Islands. *Geol. Mag.*, *135*(5), 591–604.

Chaffey, D., Cliff, R., & Wilson, B. (1989). Characterization of the St Helena magma source. *Geol. Soc. Spec. Publ.*, *42*(1), 257–276.

Clague, D. A., Dalrymple, G. B., Wright, T., Klein, F., Koyanagi, R., Decker, R., & Thomas, D. (1989). The Hawaiian-Emperor chain. In *The Eastern Pacific Ocean and Hawaii.*

Clague, D. A., Weber, W. S., & Dixon, J. E. (1991). Picritic glasses from Hawaii. *Nature*, *353*(6344), 553–556.

Cliff, R., Baker, P., & Mateer, N. (1991). Geochemistry of inaccessible island volcanics. *Chem. Geol.*, *92*(4), 251–260.

Clouard, V., & Bonneville, A. (2005). Ages of seamounts, islands, and plateaus on the Pacific plate. *Geol. Soc. Am. Spec. Pap.*, *388*, 71.

Cousens, B. L., & Clague, D. A. (2015). Shield to rejuvenated stage volcanism on Kauai and Niihau, Hawaiian Islands. *J. Petrol.*, *56*(8), 1547–1584.

Danyushevsky, L. V., & Plechov, P. (2011). Petrolog3: Integrated software for modeling crystallization processes. *Geochem. Geophys. Geosys.*, *12*(7).

Duncan, R., & Varne, R. (1988). The age and distribution of the igneous rocks of Macquarie Island. In *Papers and proceedings of the royal society of tasmania* (Vol. 122, pp. 45–50).

Duncan, R. A. (2002). A time frame for construction of the Kerguelen Plateau and

Broken Ridge. *J. Petrol.*, *43*(7), 1109–1119.

Duncan, R. A., & McDougall, I. (1974). Migration of volcanism with time in the Marquesas Islands, French Polynesia. *Earth Planet. Sci. Lett.*, *21*(4), 414–420.

Duncan, R. A., & McDougall, I. (1976). Linear volcanism in French polynesia. *J. Volcanol. Geotherm. Res.*, *1*(3), 197–227.

Dyhr, C. T., & Holm, P. M. (2010). A volcanological and geochemical investigation of Boa Vista, Cape Verde Islands: 40Ar/39Ar geochronology and field constraints. *J. Volcanol. Geotherm. Res.*, *189*(1-2), 19–32.

Esser, R. P., Kyle, P. R., & McIntosh, W. C. (2004). ^{40}Ar/^{39}Ar dating of the eruptive history of Mount Erebus, Antarctica: volcano evolution. *Bull. Volcanol.*, *66*, 671–686.

Fodor, R., Frey, F., Bauer, G., & Clague, D. (1992). Ages, rare-earth element enrichment, and petrogenesis of tholeiitic and alkalic basalts from Kahoolawe Island, Hawaii. *Contrib. Mineral. Petrol.*, *110*, 442–462.

França, Z. T., Tassinari, C. C., Cruz, J. V., Aparicio, A. Y., Araña, V., & Rodrigues, B. N. (2006). Petrology, geochemistry and Sr–Nd–Pb isotopes of the volcanic rocks from Pico Island—Azores (Portugal). *J. Volcanol. Geotherm. Res.*, *156*(1-2), 71–89.

Geist, D. J., Snell, H., Snell, H., Goddard, C., & Kurz, M. D. (2014). A paleogeographic model of the Galápagos Islands and biogeographical and evolutionary implications. *The Galápagos: a natural laboratory for the earth sciences*, 145–166.

Haase, K., Devey, C. W., Mertz, D. F., Stoffers, P., & Garbe-Schönberg, D. (1996). Geochemistry of lavas from Mohns Ridge, Norwegian-Greenland Sea: implications for melting conditions and magma sources near Jan Mayen. *Contrib. Mineral. Petrol.*,

123(3), 223–237.

Hajash, A., & Armstrong, R. L. (1972). Paleomagnetic and radiometric evidence for the age of the Comores Islands, west central Indian Ocean. *Earth Planet. Sci. Lett.*, *16*(2), 231–236.

Harris, C., Bell, J., & Atkins, F. (1983). Isotopic composition of lead and strontium in lavas and coarse-grained blocks from Ascension Island, South Atlantic—an addendum. *Earth Planet. Sci. Lett.*, *63*(1), 139–141.

Hildenbrand, A., Marques, F. O., Costa, A., Sibrant, A., Silva, P., Henry, B., . . . Madureira, P. (2012). Reconstructing the architectural evolution of volcanic islands from combined K/Ar, morphologic, tectonic, and magnetic data: The Faial Island example (Azores). *J. Volcanol. Geotherm. Res.*, *241*, 39–48.

Holm, P. M., Grandvuinet, T., Friis, J., Wilson, J. R., Barker, A. K., & Plesner, S. (2008). An ^{40}Ar-^{39}Ar study of the Cape Verde hot spot: Temporal evolution in a semistationary plate environment. *J. Geophys. Res.*, *113*(B8).

Johnson, C. L., Wijbrans, J. R., Constable, C. G., Gee, J., Staudigel, H., Tauxe, L., . . . Salgueiro, M. (1998). ^{40}Ar/^{39}Ar ages and paleomagnetism of Sao Miguel lavas, Azores. *Earth Planet. Sci. Lett.*, *160*(3-4), 637–649.

Klemme, S., & O'Neill, H. S. (2000). The near-solidus transition from garnet lherzolite to spinel lherzolite. *Contri. Mineral. Petrol.*, *138*(3), 237–248.

Leonhardt, R., McWilliams, M., Heider, F., & Soffel, H. (2009). The Gilsá excursion and the Matuyama/Brunhes transition recorded in ^{40}Ar/^{39}Ar dated lavas from Lanai and Maui, Hawaiian Islands. *Geophysical Journal International*, *179*(1), 43–58.

McKenzie, D., & O'Nions, R. K. (1995). The source regions of ocean island basalts. *J.*

Petrol., *36*(1), 133–159.

Millet, M.-A., Doucelance, R., Baker, J. A., & Schiano, P. (2009). Reconsidering the origins of isotopic variations in Ocean Island Basalts: insights from fine-scale study of São Jorge Island, Azores archipelago. *Chem. Geol.*, *265*(3-4), 289–302.

Natland, J. H., & Turner, D. L. (1985). Age progression and petrological development of Samoan shield volcanoes: evidence from K-Ar ages, lava compositions, and mineral studies. *Investigations of the Northern Melanesian Border-land, Earth Sci. Ser.*, *3*.

O'Connor, J. M., & le Roex, A. P. (1992). South Atlantic hot spot-plume systems: 1. Distribution of volcanism in time and space. *Earth Planet. Sci. Lett.*, *113*(3), 343–364.

O'Connor, J. M., & Jokat, W. (2015). Tracking the Tristan-Gough mantle plume using discrete chains of intraplate volcanic centers buried in the Walvis Ridge. *Geology*, *43*(8), 715–718.

Paul, D., White, W. M., & Blichert-Toft, J. (2005). Geochemistry of Mauritius and the origin of rejuvenescent volcanism on oceanic island volcanoes. *Geochem. Geophys. Geosys.*, *6*(6).

Putirka, K. (2008). Excess temperatures at ocean islands: Implications for mantle layering and convection. *Geology*, *36*(4), 283–286.

Recq, M., Goslin, J., Charvis, P., & Operto, S. (1998). Small-scale crustal variability within an intraplate structure: the Crozet Bank (southern Indian Ocean). *Geophys. J. Int.*, *134*(1), 145–156.

Richards, F. D., Hoggard, M. J., Crosby, A., Ghelichkhan, S., & White, N. (2020). Structure and dynamics of the oceanic lithosphere-asthenosphere system. *Phys. Earth*

Planet. Inter., *309*, 106559.

Robinson, J. A. C., & Wood, B. J. (1998). The depth of the spinel to garnet transition at the peridotite solidus. *Earth Planet. Sci. Lett.*, *164*(1-2), 277–284.

Schwarz, S., Klügel, A., & Wohlgemuth-Ueberwasser, C. (2004). Melt extraction pathways and stagnation depths beneath the Madeira and Desertas rift zones (NE Atlantic) inferred from barometric studies. *Contrib. Mineral. Petrol.*, *147*, 228–240.

Seton, M., Müller, R. D., Zahirovic, S., Williams, S., Wright, N. M., Cannon, J., . . . McGirr, R. (2020). A global data set of present-day oceanic crustal age and seafloor spreading parameters. *Geochem. Geophys. Geosys.*, *21*(10), e2020GC009214.

Stuessy, T. F., Foland, K., Sutter, J. F., Sanders, R. W., & Silva O, M. (1984). Botanical and geological significance of potassium-argon dates from the Juan Fernandez Islands. *Science*, *225*(4657), 49–51.

Tomlinson, E. L., & Holland, T. J. (2021). A thermodynamic model for the subsolidus evolution and melting of peridotite. *J. Petrol.*, *62*(1), 1–23.

Upton, B. J., Wadsworth, W., & Newman, T. (1967). The petrology of rodriguez island, indian ocean. *Geological Society of America Bulletin*, *78*(12), 1495–1506.

Vezzoli, L., & Acocella, V. (2009). Easter Island, SE Pacific: An end-member type of hotspot volcanism. *Geol. Soc. Am. Bull.*, *121*(5-6), 869–886.

Weis, D., Frey, F. A., Schlich, R., Schaming, M., Montigny, R., Damasceno, D., . . . Scoates, J. S. (2002). Trace of the Kerguelen mantle plume: Evidence from seamounts between the Kerguelen Archipelago and Heard Island, Indian Ocean. *Geochem. Geophys. Geosys.*, *3*(6), 1–27.

Workman, R. K., & Hart, S. R. (2005). Major and trace element composition of the

depleted MORB mantle (DMM). *Earth Planet. Sci. Lett.*, *231*(1-2), 53–72.
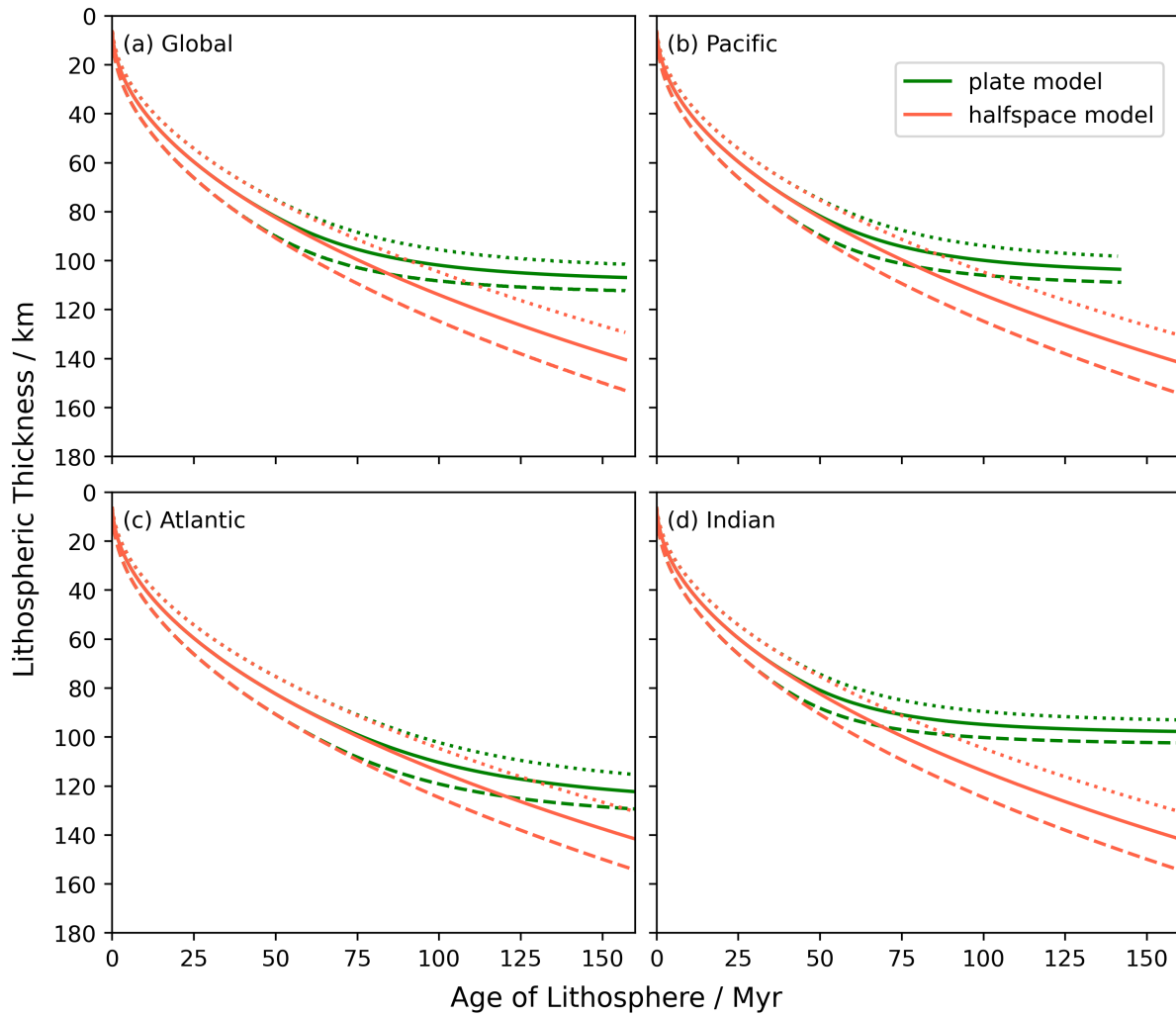
Figure S1. The world average and each oceanic basin's lithospheric thickness as a function of time for the best-fitting RHCGW20 plate model and half-space model (Richards et al., 2020). The halfspace model is coloured red, whereas the plate model is coloured green. The 1125 °C, 1175 °C, and 1225 °C contours are represented by the dotted, solid, and dashed lines, respectively.

:

Table S1. Locations of OIB samples selected from Atlantic and Indian Ocean for this study. In brackets is the name of the island chain/group to which each island belongs. The age of the lithosphere at present day and the misfit are obtained from Seton et al. (2020). The minimun and maximun eruption ages are obtained from multiple papers.

Island	Longitude	Latitude	Ocean	Lithospheric Age at Present Day (Myr)	Present-day Age Misfit (Myr)	Eruption Age Max (Myr)	Eruption Age Min (Myr)	Reference
Ascension	−14.3559	−7.9467	Atlantic	5.07	0.98	1.7	1.3	1, 2
Boa Vista (Cape Verde)	−22.8078	16.0950	Atlantic	140.78	0.67	15	4.5	3
Brava (Cape Verde)	−24.7024	14.8444	Atlantic	7.99	0.75	2	0	4
Corvo (Azores)	−31.1080	39.7023	Atlantic	10.00	0.23	1.5	1	5
Deserta	−16.5290	32.5594	Atlantic	140.99	0.24	3.6	1.7	6
Faial (Azores)	−28.6965	38.5913	Atlantic	13.52	2.00	0.85	0.03	7
Fogo (Cape Verde)	−24.3817	14.9133	Atlantic	128.52	0.63	3	0	4
Fuerteventura (Canary)	−14.0537	28.3587	Atlantic	188.36	3.77	20.6	12.5	8
Gough	−9.9353	−40.3189	Atlantic	29.70	0.37	1	0	9, 10
Gran Canaria (Canary)	−15.5474	27.9202	Atlantic	176.60	2.75	14.5	9.5	8
Inaccessible	−12.6733	−37.3004	Atlantic	20.25	0.27	6	1	11
Jan Mayen	−8.2920	71.0318	Atlantic	9.85	2.40	7	7	12
La Gomera (Canary)	−17.2194	28.1033	Atlantic	160.82	1.07	12	2.6	8
La Palma (Canary)	−17.9058	28.7134	Atlantic	154.05	0.42	2	0.1	8
Lanzarote (Canary)	−13.5900	29.0469	Atlantic	188.61	3.87	15.5	0	8
Maio (Cape Verde)	−23.1680	15.2003	Atlantic	137.97	0.21	16	6	4
Pico (Azores)	−28.3228	38.4580	Atlantic	16.05	2.40	0.3	0	5
Sal (Cape Verde)	−22.9297	16.7266	Atlantic	140.09	0.81	15	1.1	4
Santiago (Cape Verde)	−23.6205	15.0853	Atlantic	135.06	0.31	4.6	0.7	4
Sao Jorge (Azores)	−28.0303	38.6410	Atlantic	16.72	1.95	1.3	0.2	13
Sao Miguel (Azores)	−25.4970	37.7804	Atlantic	38.03	1.74	4	0.95	14, 15
St. Helena	−5.7089	−15.9650	Atlantic	40.47	1.04	9	7	16
Terceira (Azores)	−27.2206	38.7216	Atlantic	19.35	1.45	0.38	0.04	17
Tenerife (Canary)	−16.8330	28.29	Atlantic	163.66	1.33	12	7.5	8
Tristan da Cunha	−12.2777	−37.1052	Atlantic	21.66	0.27	0.21	0	9
Comoros	43.3333	−11.6455	Indian	141.23	3.14	3.65	0.01	18
Heard	73.5042	−53.0818	Indian	112.66	3.47	21	18	19
Ile aux Cochons (Crozet)	50.2315	−46.0988	Indian	72.99	0.58	0.4	0.2	20
Ile de l'Est (Crozet)	52.2197	−46.4359	Indian	70.06	0.41	8.75	2.9	20
Ile de la Possession (Crozet)	51.7378	−46.4269	Indian	70.48	0.37	5	0.5	20
Ile des Pingouins (Crozet)	50.4088	−46.4187	Indian	71.77	0.51	1.1	1.1	20, 21
Kerguelen	69.3545	−49.3948	Indian	64.84	2.67	34	0.1	20
Mauritius (Mascarene)	57.5522	−20.3484	Indian	66.13	4.05	7.8	1.9	22
Renuion (Mascarene)	55.5364	−21.1151	Indian	69.82	1.64	2.2	2	23
Rodrigues (Mascarene)	63.4272	−19.7245	Indian	13.23	0.39	1.5	1.5	24

March 28, 2024, 5:21am

Table S2. As in Table. S1 but for islands on Pacific Ocean.

Island	Longitude	Latitude	Ocean	Lithospheric Age at Present Day (Myr)	Present-day Age Misfit (Myr)	Eruption Age Max (Myr)	Eruption Age Min (Myr)	Reference
Aitutaki (Cook-Austral)	−159.7853	−18.858	Pacific	107.18	3.10	8.4	1	25, 26
Alexander Selkirk (Juan Fernandez)	−80.787	−33.761	Pacific	29.07	0.33	2.58	0.89	27
Bara Bora (Society)	−151.7415	−16.5004	Pacific	80.46	1.00	3.39	3.12	25
Darwin (Galapagos)	−92.0041	1.6787	Pacific	2.66	0.24	2	0.4	28
Easter	−109.3497	−27.1127	Pacific	6.33	1.78	0.78	0.11	29
Eiao (Marquesas)	−140.6690	−7.9790	Pacific	54.28	0.18	5.6	5.4	25, 31
Espanole (Galapagos)	−89.6722	−1.3758	Pacific	14.83	0.46	3.5	3	28
Fangataufa (Pitcairn)	−138.7427	−22.2353	Pacific	35.39	1.18	10.62	9.64	25
Fatu Hiva (Marquesas)	−138.6489	−10.4905	Pacific	50.14	0.48	1.39	1.3	25, 30
Fernandina (Galapagos)	−91.4821	−0.4124	Pacific	12.50	0.15	0.06	0.032	28
Floreana (Galapagos)	−90.4313	−1.3083	Pacific	14.64	0.28	2.3	1.5	28
Gambier (Pitcairn)	−134.9743	−23.1097	Pacific	29.48	0.37	5.63	5.16	25
Hawaii Main Island	−155.6659	19.5429	Pacific	92.92	1.96	1	0	25
Hiva Oa (Marquesas)	−139.0211	−9.7547	Pacific	50.67	0.25	2.48	1.58	25, 30
Huahine (Society)	−150.9889	−16.7883	Pacific	77.33	0.81	2.58	2.01	25
Isabela (Galapagos)	−91.1353	−0.8292	Pacific	13.51	0.15	0.8	0.5	28
Kahoolawe (Hawaii)	−156.5961	20.5552	Pacific	94.17	1.28	1.42	0.99	32
Kauai (Hawaii)	−159.5261	22.0964	Pacific	89.17	2.28	5.8	4.3	33
Lanai (Hawaii)	−156.9273	20.8166	Pacific	94.62	1.27	1.6	1.55	34
Macquarie	158.8556	−54.6208	Pacific	20.02	0.00	11.5	9.7	35
Mangaia (Cook-Austral)	−157.9166	−21.9352	Pacific	100.70	1.62	18.9	16.6	25, 26
Marchena (Galapagos)	−90.4691	0.3184	Pacific	9.71	0.66	0.8	0.6	28
Maui (Hawaii)	−156.3319	20.7984	Pacific	93.61	1.09	1.3	1.15	36
Maupiti (Society)	−152.2620	−16.4382	Pacific	82.88	1.03	4.49	3.94	25
Mehetia (Society)	−148.0669	−17.8775	Pacific	66.30	0.37	0.55	0.2	25
Molokai (Hawaii)	−157.0226	21.1444	Pacific	91.36	1.47	1.8	1.3	25
Nihoa (Hawaii)	−161.9218	23.0605	Pacific	92.20	3.64	7.5	6.9	25
Niihau (Hawaii)	−160.1575	21.8921	Pacific	90.37	2.92	5.6	5.4	33
Nuku Hiva (Marquesas)	−140.1421	−8.8605	Pacific	53.39	0.20	4.22	3.7	25, 30
Oahu (Hawaii)	−158.0001	21.4389	Pacific	89.16	1.45	3.6	2.8	25
Pinta (Galapagos)	−90.7628	0.5920	Pacific	7.94	0.43	0.8	0.7	28
Pitcairn	−128.3242	−24.3768	Pacific	20.02	1.45	0.93	0.45	25
Raivavae (Cook-Austral)	−147.6609	−23.8650	Pacific	62.28	2.46	7	4.8	25, 26
Rapa (Cook-Austral)	−144.3313	−27.5811	Pacific	54.75	0.31	4.6	4	25, 26
Rarotonga (Cook-Austral)	−159.7763	−21.2292	Pacific	102.65	2.95	1.8	1.2	25, 26
Rimatara (Cook-Austral)	−152.7500	−22.6690	Pacific	84.87	1.39	2.6	1	25, 26
Robinson Crusoe (Juan Fernandez)	−78.8580	−33.6377	Pacific	30.47	1.13	4.39	4.07	27
Ross	166.9603	−77.5247	Pacific	48.00	0.00	4	0.3	37
Rurutu (Cook-Austral)	−151.3385	−22.4801	Pacific	83.76	1.57	12	8.4	25, 26
San Cristobal (Galapagos)	−89.4364	−0.8675	Pacific	13.12	1.04	4	2.4	28
Santa Cruz (Galapagos)	−90.3372	−0.6394	Pacific	12.96	0.23	1.1	0.03	28
Savaii (Samoan)	−172.4319	−13.6598	Pacific	114.15	2.78	5	3	25
Tahiti (Society)	−149.426	−17.6509	Pacific	71.47	0.49	1.23	0.48	25
Tubuai (Cook-Austral)	−149.4500	−23.3788	Pacific	77.91	2.02	10.4	8.6	25, 26
Tutuila (Samoan)	−170.7325	−14.3258	Pacific	113.82	3.74	1.4	1	25, 38
Ua Huka (Marquesas)	−139.5484	−8.9078	Pacific	51.62	0.20	2.78	2.75	25, 30
Ua Pou (Marquesas)	−140.0804	−9.4043	Pacific	53.59	0.18	2.95	2.95	25
Upolu (Samoan)	−171.7349	−13.9134	Pacific	114.09	3.16	2.7	1.5	25, 38

March 28, 2024, 5:21am

Table S3. References for oceanic island ages from Table. S1 and S2.

Number	Reference
1	Caplan-Auerbach, Duennebier, and Ito (2000)
2	Harris, Bell, and Atkins (1983)
3	Dyhr and Holm (2010)
4	Holm et al. (2008)
5	França et al. (2006)
6	Schwarz, Klügel, and Wohlgemuth-Ueberwasser (2004)
7	Hildenbrand et al. (2012)
8	Carracedo et al. (1998)
9	O'Connor and le Roex (1992)
10	O'Connor and Jokat (2015)
11	Cliff, Baker, and Mateer (1991)
12	Haase, Devey, Mertz, Stoffers, and Garbe-Schönberg (1996)
13	Millet, Doucelance, Baker, and Schiano (2009)
14	Abdel-Monem, Fernandez, and Boone (1975)
15	Johnson et al. (1998)
16	Chaffey, Cliff, and Wilson (1989)
17	Calvert, Moore, McGeehin, and da Silva (2006)
18	Hajash and Armstrong (1972)
19	Weis et al. (2002)
20	Recq, Goslin, Charvis, and Operto (1998)
21	Camps, Henry, Prevot, and Faynot (2001)
22	R. A. Duncan (2002)
23	Paul, White, and Blichert-Toft (2005)
24	Upton, Wadsworth, and Newman (1967)
25	Clouard and Bonneville (2005)
26	R. A. Duncan and McDougall (1976)
27	Stuessy, Foland, Sutter, Sanders, and Silva O (1984)
28	Geist, Snell, Snell, Goddard, and Kurz (2014)
29	Vezzoli and Acocella (2009)
30	R. A. Duncan and McDougall (1974)
31	Caroff et al. (1995)
32	Fodor, Frey, Bauer, and Clague (1992)
33	Cousens and Clague (2015)
34	Leonhardt, McWilliams, Heider, and Soffel (2009)
35	R. Duncan and Varne (1988)
36	Clague et al. (1989)
37	Esser, Kyle, and McIntosh (2004)
38	Natland and Turner (1985)

Table S4. Mean lithospheric thickness estimates at the time of eruption for off-axis oceanic islands in the Atlantic and Indian Ocean.

Island	Ocean	Global Plate Model	Basin-based Plate Model	Seismology	Seismolgy Corrected
Ascension	Atlantic	25.92	26.05	55.98	54.18
Boa Vista (Cape Verde)	Atlantic	105.52	118.29	82.96	75.01
Brava (Cape Verde)	Atlantic	34.32	34.2	86.21	84.79
Corvo (Azores)	Atlantic	37.79	37.85	50.96	49.29
Deserta	Atlantic	105.86	119.75	92.85	89.46
Faial (Azores)	Atlantic	45.03	44.89	50.37	49.79
Fogo (Cape Verde)	Atlantic	104.97	117.68	87.31	85.46
Fuerteventura (Canary)	Atlantic	112.94	123.32	93.49	81.21
Gough	Atlantic	64.56	64.59	80.94	80.27
Gran Canaria (Canary)	Atlantic	109.93	122.58	90.67	81.53
Inaccessible	Atlantic	50.21	50.11	47.36	42.11
Jan Mayen	Atlantic	23.23	23.14	57.15	48.36
La Gomera (Canary)	Atlantic	106.73	121.62	86.04	80.17
La Palma (Canary)	Atlantic	106.71	121.59	85.26	83.92
Lanzarote (Canary)	Atlantic	116.49	124.12	93.56	87.12
Maio (Cape Verde)	Atlantic	105.16	117.83	86.29	77.55
Pico (Azores)	Atlantic	49.12	48.94	53.35	53.16
Sal (Cape Verde)	Atlantic	105.48	118.76	80.76	74
Santiago (Cape Verde)	Atlantic	105.57	118.56	85.45	83
Sao Jorge (Azores)	Atlantic	49.16	49.01	51.65	50.67
Sao Miguel (Azores)	Atlantic	70.77	70.98	68.28	65.87
St. Helena	Atlantic	67.92	67.82	81.68	75.1
Terceira (Azores)	Atlantic	53.3	53.12	57.57	57.32
Tenerife (Canary)	Atlantic	106.79	121.78	87.38	79.77
Tristan da Cunha	Atlantic	56.26	56.22	48.22	48.08
Comoros	Indian	106.04	97.25	87.73	85.61
Heard	Indian	100.51	94.1	99.31	85.4
Ile aux Cochons (Crozet)	Indian	94.78	90.24	67.32	67.02
Ile de l'Est (Crozet)	Indian	91.01	87.62	72.1	66.64
Ile de la Possession (Crozet)	Indian	92.73	89.11	70.6	68.05
Ile des Pingouins (Crozet)	Indian	93.65	90.02	67.32	66.25
Kerguelen	Indian	80.93	79.26	71.7	52.45
Mauritius (Mascarene)	Indian	89.54	86.81	76.76	72.57
Renuion (Mascarene)	Indian	92.69	88.88	84.59	82.57
Rodrigues (Mascarene)	Indian	42.77	42.89	59.93	58.26

Table S5. Mean lithospheric thickness estimates at the time of eruption for off-axis oceanic islands in the Pacific Ocean.

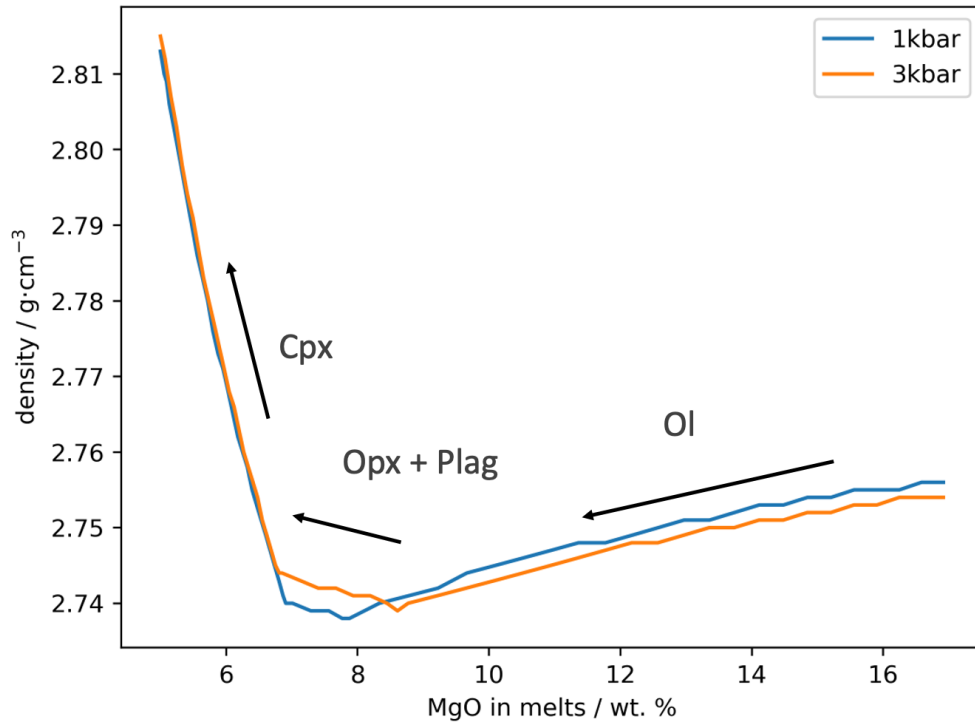| Island	Ocean	Global Plate Model	Basin-based Plate Model	Seismology	Seismolgy Corrected
Aitutaki (Cook-Austral)	Pacific	102.41	100.17	84.37	80.46
Alexander Selkirk (Juan Fernandez)	Pacific	62.68	62.54	63.91	62.1
Bara Bora (Society)	Pacific	96.4	95.13	73.34	70.41
Darwin (Galapagos)	Pacific	18.26	18.17	42.86	40.91
Easter	Pacific	31.98	32.06	44.91	44.24
Eiao (Marquesas)	Pacific	81.8	81.55	79.35	74.71
Espanole (Galapagos)	Pacific	42.67	42.5	46.28	41.28
Fangataufa (Pitcairn)	Pacific	60.39	60.5	80.94	72.44
Fatu Hiva (Marquesas)	Pacific	81.59	81.48	68	66.7
Fernandina (Galapagos)	Pacific	43.92	43.99	44.67	44.6
Floreana (Galapagos)	Pacific	44.46	44.48	46.72	43.91
Gambier (Pitcairn)	Pacific	59.28	59.4	85.15	80.74
Hawaii Main Island	Pacific	100.51	98.53	81.38	80.69
Hiva Oa (Marquesas)	Pacific	81.53	81.3	70.38	68.49
Huahine (Society)	Pacific	95.52	94.36	73.77	71.71
Isabela (Galapagos)	Pacific	44.56	44.52	45.56	44.59
Kahoolawe (Hawaii)	Pacific	100.47	98.7	73.91	72.81
Kauai (Hawaii)	Pacific	98.63	96.96	81.5	77.31
Lanai (Hawaii)	Pacific	100.71	98.81	73.91	72.49
Macquarie	Pacific	38.85	38.95	76.44	66.89
Mangaia (Cook-Austral)	Pacific	98.23	96.53	83.35	68.31
Marchena (Galapagos)	Pacific	38.22	38.29	43.46	42.36
Maui (Hawaii)	Pacific	100.26	98.59	73.93	72.82
Maupiti (Society)	Pacific	96.85	95.54	74.45	70.69
Mehetia (Society)	Pacific	91.91	90.99	75.94	75.55
Molokai (Hawaii)	Pacific	99.95	98.17	74.25	72.86
Nihoa (Hawaii)	Pacific	98.54	97.11	81.62	75.69
Niihau (Hawaii)	Pacific	98.66	97.26	84.98	80.48
Nuku Hiva (Marquesas)	Pacific	82.41	82	74.98	71.47
Oahu (Hawaii)	Pacific	98.9	97.34	80.66	77.94
Pinta (Galapagos)	Pacific	34.75	34.71	43.19	42
Pitcairn	Pacific	53.36	53.62	54.35	53.5
Raivavae (Cook-Austral)	Pacific	86.64	86.27	73.62	68.23
Rapa (Cook-Austral)	Pacific	82.81	82.59	68.14	63.91
Rarotonga (Cook-Austral)	Pacific	102.13	100.09	84.42	82.83
Rimatara (Cook-Austral)	Pacific	98.3	96.74	71.62	69.96
Robinson Crusoe (Juan Fernandez)	Pacific	61.59	61.59	64.11	59.64
Ross	Pacific	79.49	79.24	59.08	56.62
Rurutu (Cook-Austral)	Pacific	94.89	94.09	72.2	62.33
San Cristobal (Galapagos)	Pacific	39.81	39.9	44.73	39.61
Santa Cruz (Galapagos)	Pacific	43.86	43.88	45.38	44.52
Savaii (Samoan)	Pacific	103.4	101.19	71.48	67.74
Tahiti (Society)	Pacific	93.77	92.91	74.35	73.56
Tubuai (Cook-Austral)	Pacific	92.91	92.17	73.24	64.29
Tutuila (Samoan)	Pacific	103.73	101.52	81.67	80.46
Ua Huka (Marquesas)	Pacific	81.83	81.6	73.76	71.28
Ua Pou (Marquesas)	Pacific	82.92	82.84	74.4	71.77
Upolu (Samoan)	Pacific	103.61	101.32	73.65	71.77

Figure S2. Magma density v.s. MgO content, calculated from Petrolog3 (Danyushevsky & Plechov, 2011), from fractionation at 1 and 3 kbar, respectively. The fractional crystallisation model is taken from Ariskin et al. (1993). Olivine crystallises first, then othropyroxene and plagioclase. Clinopyroxene forms at last. The primary magma composition is taken from Clague et al. (1991).
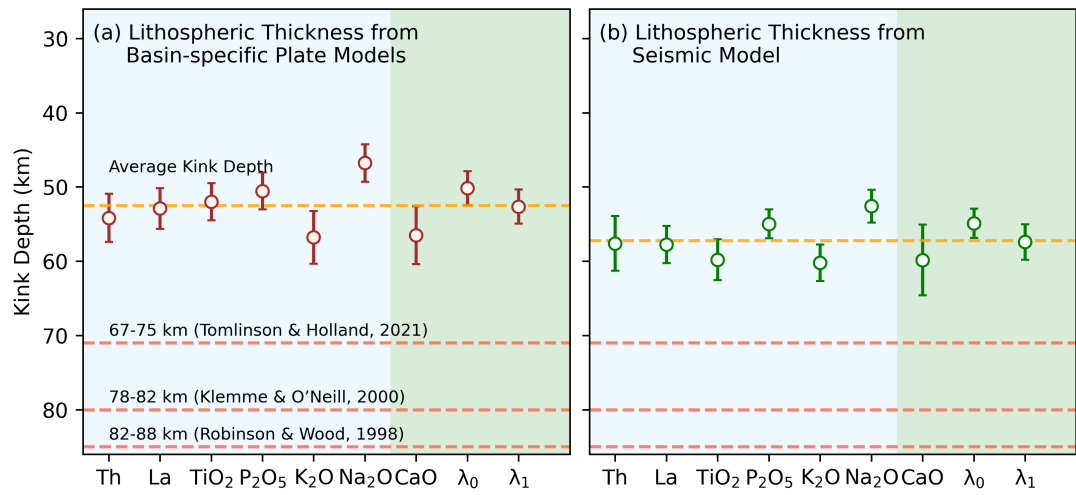
Figure S3. Preferred kink depths for geochemical parameters that are optimally fitted by bi-linear models. Circles with errors = mean and uncertainty range, where the error is equal to two standard deviations of likely kink depths. (a) Results for lithospheric thickness estimates obtained from basin-specific plate models; orange dashed line = average kink depth; red dashed lines = near-solidus spinel-garnet transition depths from experimental petrology (Robinson & Wood, 1998; Klemme & O'Neill, 2000; Tomlinson & Holland, 2021); blue shading = bi-linear trends dominated by melt-fraction effects; green shading = bi-linear trends affected by a combination of melt fraction and spinel-garnet transition depth. (b) Same for lithospheric thicknesses estimated from seismic tomography.
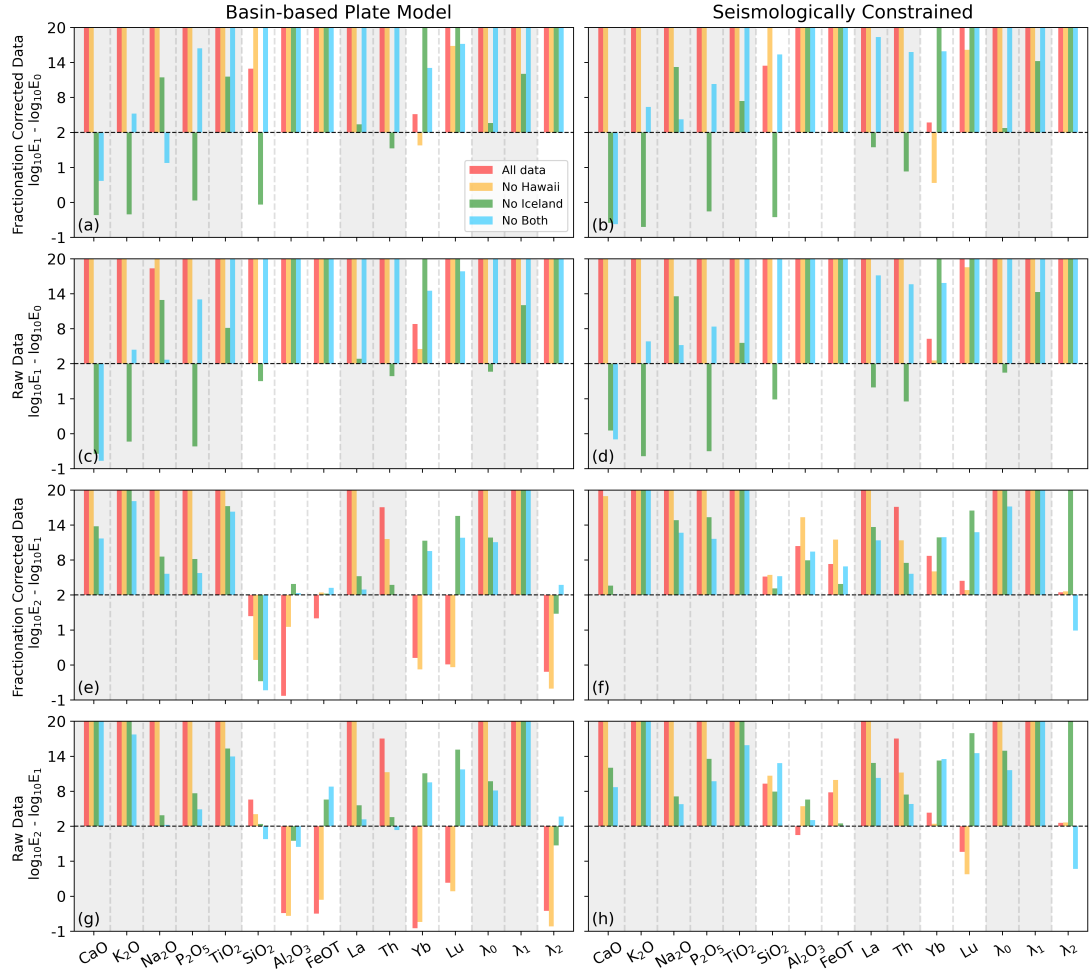
Figure S4. (a-d) $\log_{10}E_1 - \log_{10}E_0$ and (e-f) $\log_{10}E_2 - \log_{10}E_1$ values for major, trace elements and λs in OIBs, using all data (red) as well as datasets with Iceland samples removed (orange), Hawaii samples removed (green), and both sample sets removed (blue). Data in panels (a, b, e, f) are raw OIB compositions and data in panel (c, d, g, h) are fractionation corrected. Lithospheric thickness is estimated using the basin-based plate model (left column) and seismic data (right column). The key threshold value of 2 is represented by dashed horizontal lines, meaning that if the evidence difference of two models is larger than 2, the first model is statistically more favourable. For illustrative purposes, evidence values exceeding 20 are capped. When including all data, using basin-specific plate models and applying fractionation correction, parameters shaded in grey are best fitted by bi-linear models, and parameters without shading are best fitted by bi-linear models. March 28, 2024, 5:21am

Figure S5. As in Figure S4 but lithospheric thickness is estimated using the global plate model (left column) and seismic data corrected for re-thickening (right column).
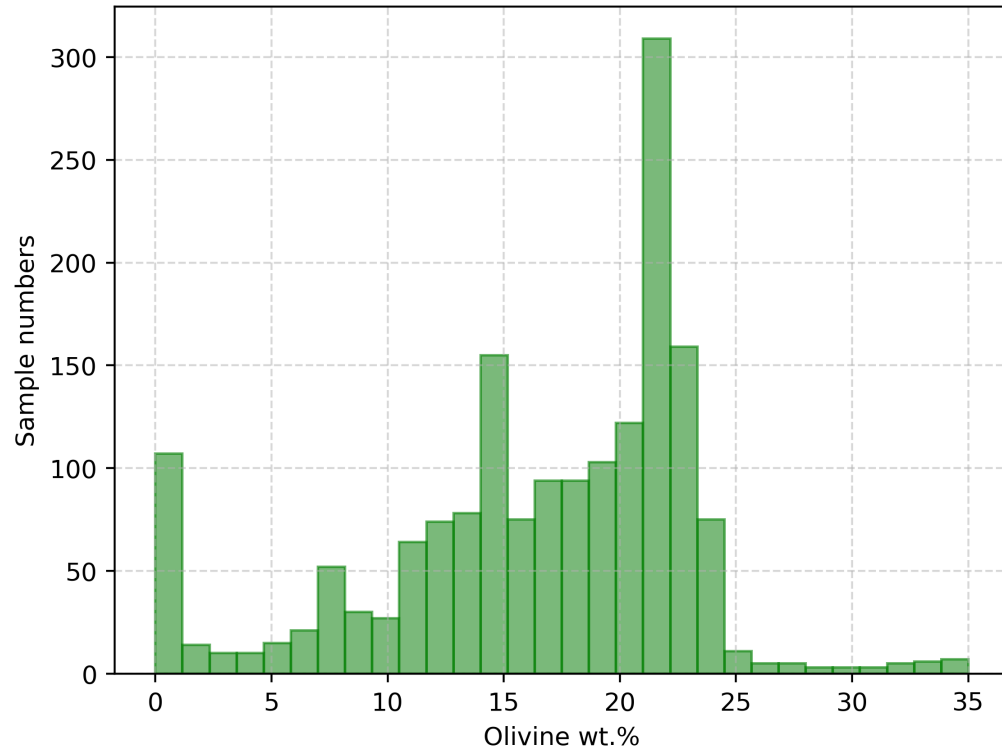
Figure S6. The predicted fraction of olivine that has crystallised from the primitive magma to form the observed OIB compositions. Calculation is performed in Petrolog3 (Danyushevsky & Plechov, 2011).
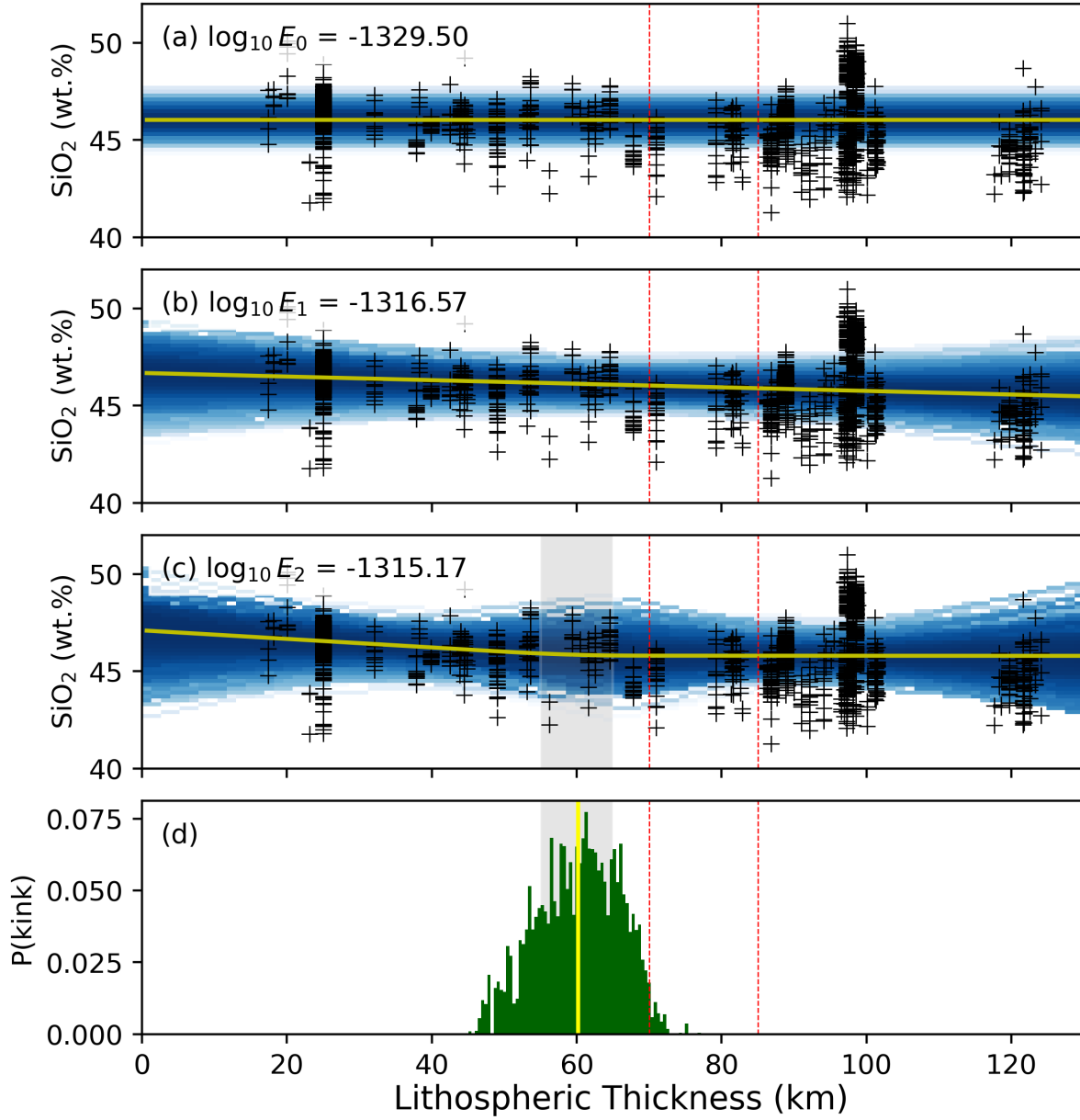
Figure S7. Statistical evidence evaluation results for SiO$_2$ data, including all sample clusters, using the basin-based plate model, and corrected for the impact of fractional crystallisation. Fitting results are obtained using: (a) a constant model; (b) a linear model; and (c) a bi-linear model. The mean curve is represented by the yellow line, with probability density indicated via blue shading. Panel (d) shows a histogram of the depth of the breakpoint in the bi-linear model, with the yellow vertical line indicating the mean value.
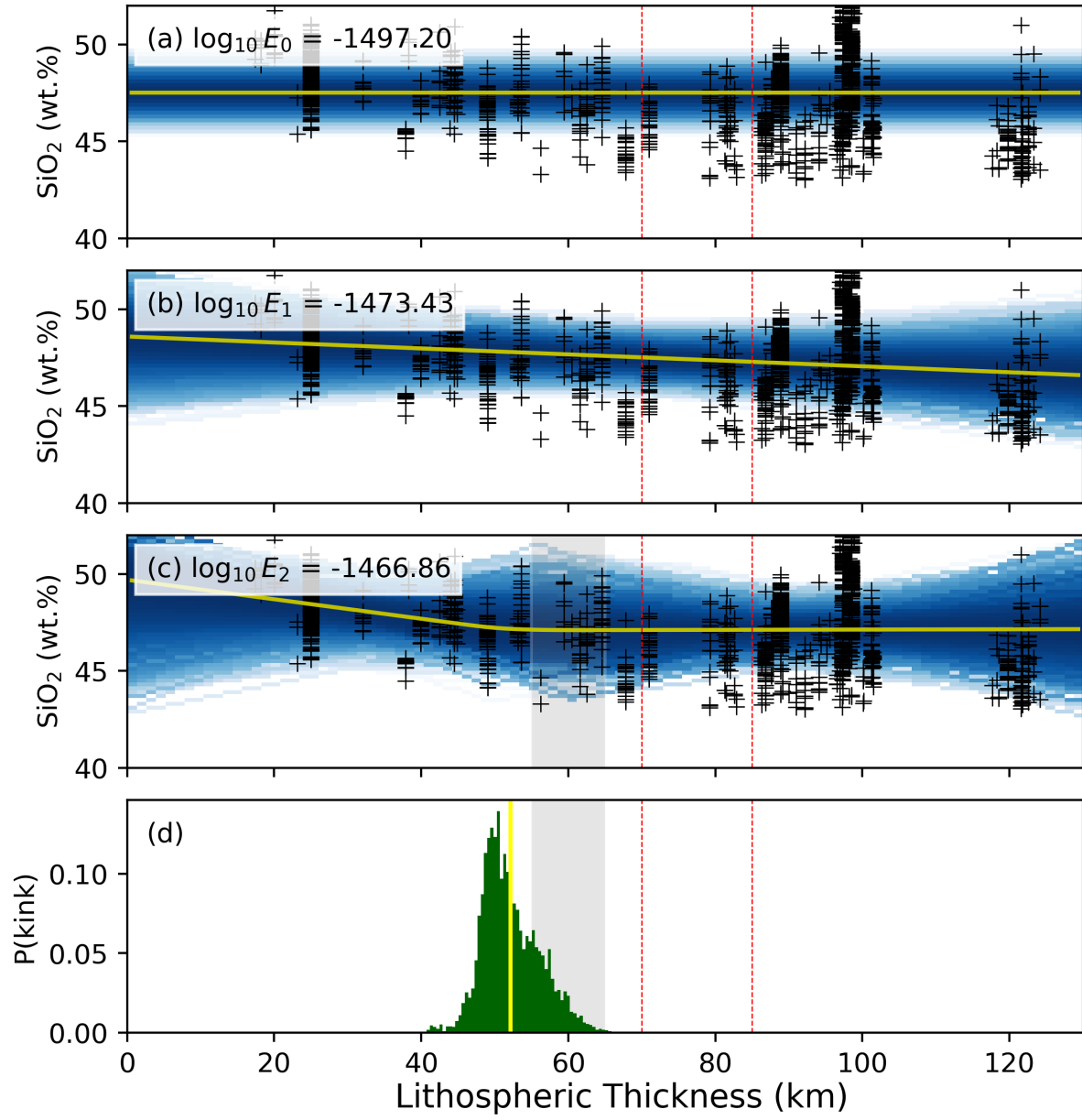
March 28, 2024, 5:21am

Figure S8. As in Figure S7 but for non-fractionation corrected SiO$_2$ dataset.

Figure S9. Statistical evidence evaluation results for incompatible elements, but excluding Icelandic and Hawaii samples. Data and panel contents same as for Figure 9 in the main text.

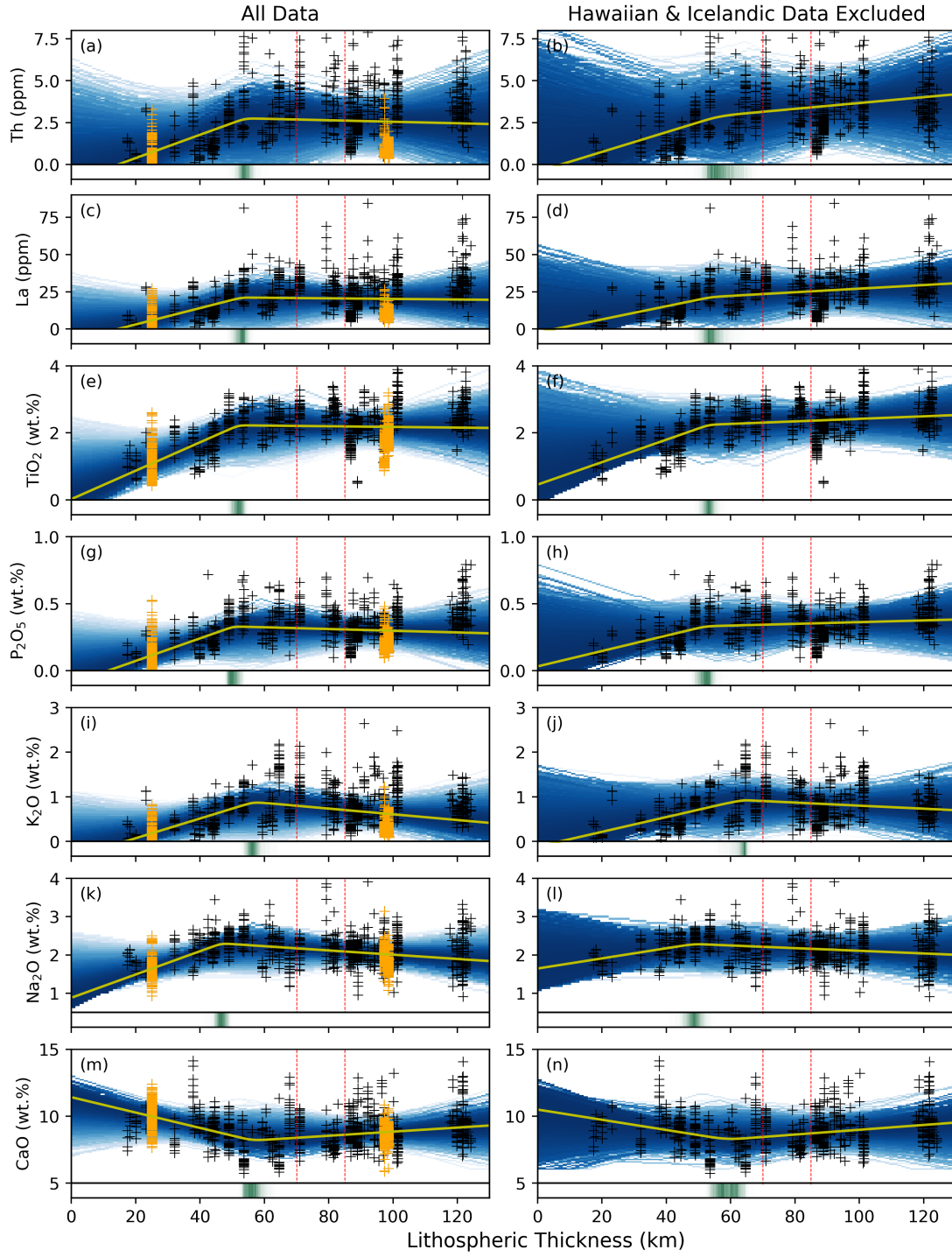**Figure S10.** Statistical evidence evaluation results for incompatible elements, but excluding Icelandic and Hawaii samples. Data and panel contents same as for Figure 9 in the main text.

:

Figure S11. The relationship between lithospheric thickness and the potential temperature of OIB sources estimated from geochemical constraints of (a) Putirka (2008), (b) Bao et al. (2022) and (c) Ball et al. (2021). Localities in the Atlantic, Pacific and Indian Oceans are represented by green, blue and red circles, respectively.

Table S6. λ_2 values for a two-phase melting model at different F_{grt}, F_{spl} and starting melting pressure. REE concentrations in primitive mantle are from McKe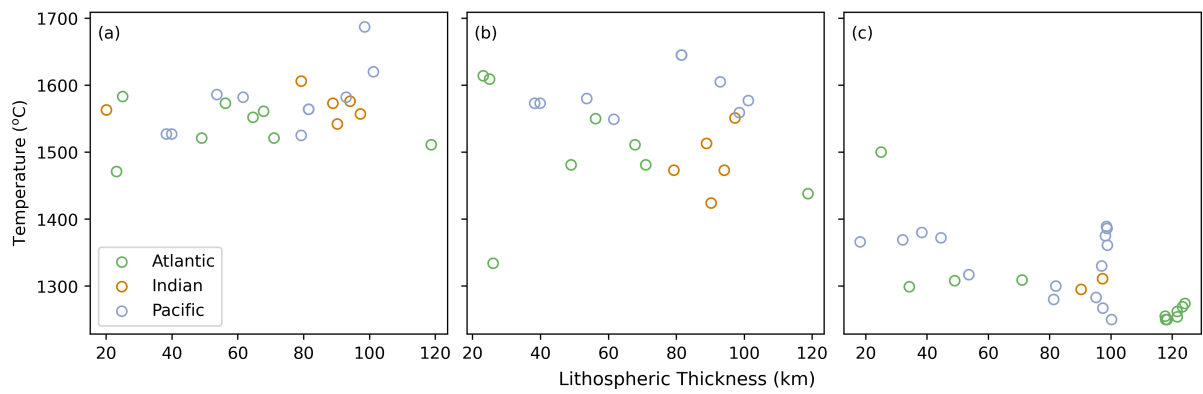nzie and O'Nions (1995), and REE concentrations in depleted mantle are from Workman and Hart (2005). Python scripts are available online, as indicated in the Open Research Section.

F_{grt} \ F_{spl}	0.00	0.01	0.02	0.03	0.04	0.05	0.06	0.07	0.08	0.09	0.00	0.01	0.02	0.03	0.04	0.05	0.06	0.07	0.08	0.09
3 GPa						Primitive										Depleted				
0.00	–	27.34	22.00	17.40	13.49	10.22	7.52	5.29	3.46	1.98	–	16.36	11.02	6.42	2.51	-0.76	-3.47	-5.70	-7.52	-9.00
0.01	14.09	16.84	14.27	11.29	8.55	6.18	4.20	2.55	1.20	0.10	3.10	5.86	3.29	0.31	-2.43	-4.80	-6.79	-8.43	-9.78	-10.88
0.02	9.54	10.43	8.76	6.69	4.74	3.03	1.59	0.39	-0.59	-1.38	-1.45	-0.55	-2.23	-4.29	-6.24	-7.95	-9.39	-10.59	-11.57	-12.37
0.03	5.78	5.90	4.68	3.22	1.83	0.60	-0.43	-1.29	-1.98	-2.54	-5.20	-5.08	-6.30	-7.76	-9.16	-10.38	-11.42	-12.27	-12.97	-13.52
0.04	2.80	2.59	1.67	0.62	-0.37	-1.24	-1.97	-2.57	-3.04	-3.41	-8.18	-8.39	-9.31	-10.36	-11.36	-12.22	-12.95	-13.55	-14.02	-14.39
0.05	0.54	0.19	-0.52	-1.28	-1.99	-2.59	-3.10	-3.50	-3.80	-4.02	-10.45	-10.79	-11.50	-12.27	-12.97	-13.58	-14.08	-14.48	-14.78	-15.01
0.06	-1.07	-1.47	-2.04	-2.61	-3.11	-3.53	-3.87	-4.13	-4.31	-4.42	-12.05	-12.46	-13.02	-13.59	-14.09	-14.52	-14.85	-15.11	-15.29	-15.40
0.07	-2.09	-2.52	-3.00	-3.44	-3.81	-4.11	-4.33	-4.49	-4.58	-4.62	-13.07	-13.51	-13.98	-14.42	-14.79	-15.09	-15.32	-15.47	-15.56	-15.60
0.08	-2.56	-3.04	-3.47	-3.84	-4.14	-4.36	-4.52	-4.61	-4.64	-4.63	-13.55	-14.02	-14.45	-14.82	-15.12	-15.34	-15.50	-15.59	-15.63	-15.61
0.09	-2.54	-3.06	-3.50	-3.85	-4.12	-4.31	-4.43	-4.49	-4.50	-4.47	-13.52	-14.04	-14.48	-14.83	-15.10	-15.29	-15.41	-15.48	-15.49	-15.45
4 GPa																				
0.00	–	27.86	22.70	18.21	14.37	11.13	8.42	6.17	4.31	2.78	–	16.87	11.72	7.23	3.39	0.15	-2.56	-4.81	-6.67	-8.20
0.01	-2.20	17.22	15.33	12.43	9.68	7.26	5.21	3.50	2.08	0.91	-13.18	6.24	4.34	1.45	-1.30	-3.72	-5.77	-7.48	-8.90	-10.07
0.02	-7.50	8.64	8.90	7.36	5.57	3.89	2.42	1.18	0.14	-0.72	-18.48	-2.34	-2.08	-3.62	-5.42	-7.09	-8.56	-9.80	-10.84	-11.70
0.03	-12.08	1.86	3.49	3.01	2.02	0.98	0.01	-0.83	-1.54	-2.13	-23.06	-9.12	-7.49	-7.97	-8.96	-10.01	-10.97	-11.82	-12.52	-13.11
0.04	-15.97	-3.57	-1.03	-0.68	-1.01	-1.53	-2.07	-2.57	-3.00	-3.35	-26.95	-14.55	-12.01	-11.66	-11.99	-12.51	-13.05	-13.55	-13.98	-14.33
0.05	-19.24	-7.95	-4.79	-3.80	-3.59	-3.68	-3.86	-4.07	-4.25	-4.39	-30.22	-18.94	-15.77	-14.79	-14.57	-14.66	-14.84	-15.05	-15.23	-15.38
0.06	-21.95	-11.52	-7.92	-6.44	-5.79	-5.51	-5.40	-5.35	-5.33	-5.29	-32.93	-22.50	-18.91	-17.42	-16.77	-16.50	-16.38	-16.34	-16.31	-16.28
0.07	-24.19	-14.43	-10.54	-8.66	-7.66	-7.08	-6.72	-6.46	-6.25	-6.06	-35.17	-25.41	-21.52	-19.65	-18.65	-18.07	-17.70	-17.44	-17.23	-17.04
0.08	-26.02	-16.81	-12.71	-10.54	-9.26	-8.42	-7.84	-7.39	-7.03	-6.70	-37.00	-27.79	-23.70	-21.52	-20.24	-19.41	-18.82	-18.38	-18.01	-17.68
0.09	-27.50	-18.76	-14.53	-12.12	-10.60	-9.56	-8.79	-8.19	-7.68	-7.24	-38.49	-29.75	-25.51	-23.11	-21.59	-20.54	-19.77	-19.17	-18.66	-18.22
5 GPa																				
0.00	–	28.37	23.43	19.09	15.34	12.13	9.43	7.15	5.25	3.67	–	17.39	12.44	8.10	4.35	1.15	-1.56	-3.83	-5.73	-7.31
0.01	-3.11	19.25	17.01	13.95	11.08	8.57	6.43	4.62	3.12	1.86	-14.09	8.26	6.02	2.97	0.10	-2.41	-4.55	-6.36	-7.87	-9.12
0.02	-8.25	11.13	11.06	9.24	7.23	5.38	3.76	2.38	1.22	0.26	-19.24	0.14	0.07	-1.75	-3.75	-5.60	-7.22	-8.60	-9.76	-10.72
0.03	-12.78	4.41	5.84	5.07	3.83	2.56	1.41	0.41	-0.44	-1.15	-23.77	-6.57	-5.14	-5.91	-7.16	-8.42	-9.57	-10.57	-11.42	-12.13
0.04	-16.72	-1.13	1.36	1.44	0.85	0.09	-0.65	-1.32	-1.90	-2.38	-27.70	-12.11	-9.62	-9.55	-10.14	-10.89	-11.64	-12.31	-12.88	-13.37
0.05	-20.10	-5.72	-2.47	-1.71	-1.75	-2.07	-2.46	-2.84	-3.18	-3.46	-31.08	-16.71	-13.45	-12.69	-12.73	-13.05	-13.44	-13.82	-14.16	-14.45
0.06	-22.98	-9.55	-5.74	-4.42	-4.00	-3.95	-4.04	-4.17	-4.30	-4.40	-33.96	-20.53	-16.72	-15.40	-14.99	-14.93	-15.02	-15.15	-15.28	-15.39
0.07	-25.42	-12.74	-8.52	-6.76	-5.96	-5.59	-5.41	-5.32	-5.27	-5.22	-36.40	-23.73	-19.51	-17.74	-16.94	-16.57	-16.39	-16.31	-16.25	-16.20
0.08	-27.47	-15.43	-10.90	-8.77	-7.65	-7.01	-6.61	-6.33	-6.11	-5.92	-38.46	-26.41	-21.88	-19.76	-18.64	-17.99	-17.59	-17.31	-17.09	-16.90
0.09	-29.20	-17.68	-12.93	-10.51	-9.12	-8.24	-7.64	-7.19	-6.83	-6.51	-40.19	-28.66	-23.91	-21.49	-20.10	-19.22	-18.62	-18.17	-17.81	-17.50

March 28, 2024, 5:21am